Novel method to synthesize highly ordered ethane-bridged PMOs under mild acidic conditions : taking advantages of phosphoric acid

Reference:

Lin Feng, Meng Xiangyan, Kukueva Elena, Kus Monika, Mertens Myriam, Bals Sara, Van Doorslaer Sabine, Cool Pegie.- Novel method to synthesize highly ordered ethane-bridged PMOs under mild acidic conditions : taking advantages of phosphoric acid Microporous and mesoporous materials: zeolites, clays, carbons and related materials - ISSN 1387-1811 - 207(2015), p. 61-70
DOI: http://dx.doi.org/doi:10.1016/j.micromeso.2014.12.029

Novel method to synthesize highly ordered ethane-bridged PMOs under mild acidic conditions: taking advantages of phosphoric acid

Feng Lin,[1,2] Xiangyan Meng,[1] Elena Kukueva,[1,4] Monika Kus,[1] Myrjam Mertens,[3] Sara Bals,[4] Sabine Van Doorslaer,[2] and Pegie Cool[1*]

1. Laboratory of Adsorption and Catalysis, Department of Chemistry, University of Antwerp, Universiteitsplein 1, B-2610, Wilrijk, Belgium.

2. Laboratory of Biomedical Physics, Department of Physics, University of Antwerp, Universiteitsplein 1, B-2610, Wilrijk, Belgium.

3. Flemish Institute for Technological Research, VITO, Boerentang 200, B-2400,Mol, Belgium

4. EMAT, Department of Physics, University of Antwerp, Groenenborgerlaan 171, B-2020 Antwerp, Belgium.

Corresponding Author

* Fax: +32 3 2652374; Tel: : +32 3 2652355; E-mail: pegie.cool@uantwerpen.be

Abstract

Highly ordered SBA-15-type ethane-bridged PMOs have been obtained by employing H_3PO_4 as acid to tune the pH in the presence of copolymer surfactant P123. The effects of the acidity and the addition of inorganic salt on the formation of the mesostructure are investigated. It is found that, compared with HCl, the polyprotic weak acid H_3PO_4 is preferable for the synthesis of highly ordered SBA-15-type ethane-bridged PMOs with larger pore size and surface areas under mild acidic conditions. Moreover, taking the advantages of the mild acidic condition, vanadium-containing SBA-15-type ethane-bridged PMOs were successfully prepared through a direct synthesis approach. The XRD, N_2-sorption, UV-Vis and CW-EPR studies of the V-PMO show that part of the vanadium species are present in polymeric $(V–O–V)_n$ clusters, while part of the vanadium centers are well-dispersed and immobilized on the inner surface of the mesopores.

Keywords: SBA-15-type ethane-bridged PMOs; H_3PO_4; mild acidic condition; vanandium-containing ethane-bridged PMOs; EPR

1. Introduction

Periodic mesoporous organosilicas (PMOs) form a new class of mesoporous materials with highly ordered pore structures and uniformly distributed organic groups inside the siliceous frameworks.[1-4] The combination of the organic and inorganic components gives PMOs some unique properties, such as the tunable surface hydrophobicity, and enhanced mechanical and hydrothermal stability[5]. Moreover, the porous structure, and surface and framework properties of PMO materials can be finely tuned by varying the bridging organic groups and the synthesis conditions. So far, a variety of organic groups has been incorporated into the framework of PMOs, leading to materials with promising applications in many fields, such as the chemical industry (catalysis), environmental applications (metal scavenging) and medical applications (controlled drug release).

In general, PMOs are prepared via the hydrolysis and condensation of bridged silsesquioxane species $(RO)_3Si\text{-}R\text{-}Si(OR)_3$ under basic or acidic conditions in the presence of various structure-directing agents. Most PMOs reported so far have MCM-41- or SBA-15-type mesostructures consisting of uniform one-dimensional channels.[6] In comparison with the MCM-41-type PMOs synthesized with ionic alkylammonium surfactants, SBA-15-type PMOs templated by triblock copolymers surfactant are much more desirable, not only because of the larger pore size and thicker pore walls, but also due to the presence of the unique interconnected pores. Up to now, great effort has been devoted to the preparation of SBA-15-type PMOs. However, due to the different interfacial energy between the precursor and template for silica and organosilica, a precise control of the synthesis conditions is needed for obtaining highly ordered SBA-15-type PMOs in contrast to the easier fabrication of SBA-15 materials. The effect of the SiO_2/template ratio on the properties of the material has been studied by several research groups.[7, 8] Bao *et*

al.[9, 10] investigated the influence of acid concentration on the degree of structural order and the external morphology of the final product. Burleigh *et al*.[11] prepared a series of SBA-15-type PMOs with different pore diameter (from 6 to 20 nm) by using 1,3,5-trimethylbenzene (TMB) as the swelling agent. Moreover, the structural order and morphology of these materials could be strongly affected by the addition of additives such as inorganic salts.[12-14] Up to now, in most cases, SBA-15-type PMOs are synthesized at a pH<1 using strong acids, like HCl. To our knowledge, there is no report on the synthesis of SBA-15-type PMOs using weak acids. Compared with HCl, H_3PO_4 is a polyprotic weaker acid, and it has been reported for SBA-15 that the use of H_3PO_4 rather than HCl during the self-assembly process could promote changes in the ionic strength and pH at the interface.[15] Using the triblock copolymers surfactant, the self-assembly is governed by weak van der Waals interactions or hydrogen bondings. Hence, tiny modifications of the experimental conditions can lead to significant changes during the self-assembly process and consequently influence the characteristics of the final material. Colilla *et al*.[16] found that the surface area of SBA-15 can be increased by employing H_3PO_4 as an acid source. Moreover, phosphorus has been successfully incorporated into the framework when a large amount of H_3PO_4 is used. Pitchumani *et al*.[17] obtained a broader variety of morphology of SBA-15 when using H_3PO_4 compared with that of HCl. In addition, the use of the polyprotic weak acid H_3PO_4 may induce a mild acidic condition, which can be beneficial for the incorporation of metal atoms into the framework of PMO materials.

Vanadium-containing mesoporous materials have been proven to be effective catalysts for many selective oxidation reactions.[18-20] The catalytic activity and selectivity of these vanadium-containing catalysts strongly depends on the nature, location and dispersion of the vanadia in the catalyst.[20, 21] Although vanadium-containing mesoporous materials have received

considerable attention, the reports on the direct-synthesis of vanadium-containing PMO materials are still very limited. Singh *et al.*[22] have prepared vanadium-containing ethane-bridged PMOs using cationic surfactants under basic conditions. Furthermore, it was found that vanadium-containing PMOs were highly active and more stable than conventional vanadosilicates during the liquid-phase epoxidation reaction of styrene using aqueous H_2O_2 or TBHP as the oxidants.[22] Recently, a novel type of PMO material embedded with $[VO(acac)_2]$ has been successfully synthesized through a co-condensation method under basic conditions.[23] Nevertheless, all these vanadium-containing PMOs were obtained under basic conditions in the presence of cationic surfactants.

In the present study, we present the synthesis of SBA-15-type ethane-bridged PMOs by employing H_3PO_4. The effects of the acidity and inorganic salt on the formation of the mesostructure are investigated. Moreover, vanadium-containing SBA-15-type PMOs were successfully prepared through a direct synthesis approach. This is the first example of V-PMO synthesized under acidic conditions using non-ionic surfactants. In comparison to the HCl-assisted synthetic pathway, the use of H_3PO_4 is more advantageous for the formation of SBA-15-type ethane-bridged PMOs under mild acidic conditions, both from the point of view of metal incorporation and the structural properties of the final materials.

2. Experimental section

2.1 Materials

All starting materials were used as purchased without further purification: 1,2-bis(triethoxysilyl)-ethane (BTEE, 96% Sigma-Aldrich), Pluronic P123 triblock copolymer (EO_{20}-PO_{70}-EO_{20},

Sigma-Aldrich), H_3PO_4 (85% Acros Organic), HCl (37% Acros Organic), methanol (99.9% Merck KGaA), NaCl (Sigma-Aldrich), $VOSO_4 \cdot 5H_2O$ (Sigma-Aldrich)

2.2 Synthesis of PMO materials

SBA-15-type ethane-bridged PMOs were synthesized from BTEE in the presence of P123 under low acidic conditions, adapting slightly the HCl-based synthesis procedure reported by Bao *et al*.[9] In a typical synthesis procedure (***PMO 1-7***), 1.04 g P123 was dissolved in 31.5 g of H_3PO_4 solution with a definite concentration (see Table 1). Then, 2 ml BTEE was added into the above mixture at 40 ºC and stirred at the same temperature for 24 hours. The mixture was then transferred into an autoclave and followed by aging at 100 ºC under static condition for another 5 days. The obtained white precipitate was filtered, washed thoroughly with deionized water, and dried at room temperature. Surfactant template removal was accomplished by two solvent extraction cycles with ethanol. Typically, 1 g of as-made PMOs was treated under vigorous stirring for 6 h at 60 ºC in 200 ml of ethanol, followed by filtration, washing with ethanol and drying. ***PMO 8-10*** were synthesized under the same pH value with ***PMO 2-5***, but using HCl instead of H_3PO_4. ***PMO 11-13*** were prepared using H_3PO_4 with the assistance of NaCl with the molar ratios of NaCl/BTEE = 8. ***V-PMO*** was synthesized with the same recipe of ***PMO 11***, except for the addition of the vanadium source with the molar ratios of $VOSO_4$/BTEE=0.06. Table 1 lists the details of the synthesis conditions including the pH value and reactant compositions.

Table 1. *Synthetic details of the PMOs under study*

2.3 Characterization

N_2 adsorption–desorption isotherms were obtained at liquid N_2 temperature (77 K) using a Quantachrome Quadrasorb-SI automated gas adsorption system. Prior to adsorption, the samples were outgassed under high vacuum for 16 hours at 100 ºC. The specific surface area was calculated using the Brunauer-Emmet-Teller (BET) method, between a relative pressure of 0.05 and 0.35. The pore size distributions (PSD) were deduced from both the adsorption branch and desorption branch of the isotherms using the NLDFT method. The total pore volumes were calculated from the amount of N_2 vapor adsorbed at a relative pressure of 0.95. The micropore area and volume were calculated by the *t*-plot method using experimental points at a relative pressure of $P/P_0 = 0.25–0.55$.

X-ray diffraction (XRD) measurements were recorded on a Pananalytical X'PERT PRO MPD diffractometer with filtered CuKα-radiation. The measurements were performed in the 2θ mode using a bracket sample holder with a scanning speed of 0.04°/4 s in continuous mode. The unit cell parameters (*a*) were determined from the interplanar spacing of the (100) planes .

Scanning Electron Microscopy (SEM) has been performed using a JSEM 5510 system, operating at an accelerating voltage between 20–30 kV. The samples were attached to a carbon tape and sputtered with a thin gold film to minimize the charging effects. For the transmission electron microscopy (TEM) measurements, the samples were dispersed in ethanol, crushed in an agate mortar and deposited on a carbon coated copper grid. TEM images and selected area electron diffraction (SAED) were acquired using and FEI Tecnai instrument operated at 200 kV with camera length 4 m.

UV–vis diffuse reflectance spectra were recorded on a Thermo-electron evolution 500 UV–vis spectrometer equipped with a Thermo-electron RSA-UC40 diffuse reflectance cell. The average of three scanning cycles was taken with a scanning speed of 120 nm/min and a bandwidth of 2 nm. Samples were mixed with KBr to 2 wt.%.

X-band CW-EPR measurements were performed on a Bruker ESP 300E instrument, equipped with a liquid helium cryostat (Oxford Inc.), working at a microwave (mw) frequency of about 9.5 GHz. A microwave power of 1 mW, modulation frequency of 100 kHz and modulation amplitude of 0.5 mT were applied. The EasySpin program[24] was utilized to simulate the CW-EPR spectra.

3. Results and discussion

Influence of the acidity on the formation of SBA-15-type ethane-bridged PMOs

Figure 1. *XRD patterns of ethane-bridged PMOs synthesized at different pH value ranging from 2.0 to 0.5 (PMO-2 to PMO-7 in Table 1). A: as-synthesized samples, B: solvent-extracted samples.*

Figure 1 shows the XRD patterns of SBA-15-type ethane-bridged PMOs synthesized with H_3PO_4 at different acidity. For the sample synthesized with pH=2.1 (PMO-1), no precipitation occurred, indicating that the acid concentration is too low for the formation of an ordered structure. For pH values from 1.5 to 2.0, the XRD patterns of the as-synthesized sample exhibit well-resolved peaks which can be assigned to the (100), (110) and (200) reflections of a highly ordered 2D hexagonal symmetry (*p6mm*) (Figure 1). However, further decrease of the pH value resulted in a less ordered structure, which is evidenced by the dramatically decreased intensity of the (100) peak and the poorly resolved higher order peaks. This suggests that the very strong acidic conditions do not favor formation of highly ordered ethane-bridged PMOs. A previous study already showed that the highly ordered mesoporous structure of PMOs is difficult to achieve at

high HCl conditions without NaCl assistance.[13] In contrast, for the synthesis of SBA-15 using H_3PO_4, a higher acid concentration is favored for the formation of more ordered 2-D hexagonal mesostructure.[16] It is known that the formation of mesosilicas in the presence of P123 as surfactant is mainly due to the interaction between the ethylene oxide (EO) moieties of P123 and the protonated hydroxyl groups of the hydrolyzed silica precursor. Because of the organic bridging units within the organosilica precursor, the use of an organosilica precursor results in less hydroxyl groups compared to the use of a pure silica precursor. Consequently, the self-assembly of the mesostructure is relatively poor in the organosilica synthetic system. In this case, a slower condensation will provide enough time for the self-assembly process to reinforce the polymerization of the silica species and the cross-linked organosilica network[9]. The hydrolysis and condensation rate of the organosilica precursor is proportional to the acidity of the synthetic system. Therefore, during the synthesis of ethane-bridged PMOs, lowering the acid concentration is an effective way to slow down the reaction rate, resulting in a better mesostructure. However, after solvent extraction, only one broad peak can be observed in the XRD pattern of PMO-2 (pH=2), indicating a disordered mesostructure (Figure 1B). Considering its well-resolved XRD pattern before solvent extraction, this result indicates that the well-ordered mesostructure has collapsed during the template removal process. The other PMOs retain their order upon template removal.

Table 2. *Structural parameters of ethane-bridged PMOs under study*

Figure 2. *(left) N_2 adsorption-desorption isotherms of ethane-bridged PMOs synthesized at different pH ranging from 2.0 to 0.5 (PMO-2 to PMO-7 in Table 1) and (right) corresponding pore-size distributions.*

The nitrogen adsorption-desorption isotherms of the ethane-bridged PMOs prepared with different acidity are shown in Figure 2. All the isotherms, except for those of PMO-2, are of type

IV according to IUPAC classification and exhibited an H1 hysteresis loop, which is typical for mesoporous materials with cylindrical channels. The sharp increase of the adsorbed volume at P/P_0=0.60~0.65 due to the N_2 capillary condensation indicates the uniformity of the mesopores, which was also confirmed by the narrow peak of the NLDFT pore-size distribution curve. It can be noticed that with the decrease of the pH value, the pore size of the PMOs gradually decreases, whereas the pore wall thickness gradually increases (table 2). The decreased pore size can be explained by the fact that the protonation of the EO moieties at higher acidity can increase the hydrophilic volume and accordingly decrease the hydrophobic core volume of the micelles that determine the structure of the mesopores.[12] In addition, the higher acidity will result in a faster condensation rate, which leads to a thicker pore wall in the final product. The N_2 adsorption-desorption isotherm of PMO-2 is intermediate between type I and IV, characteristic of supermicroporous-like materials.[25] Its micropore volume is 0.195 cm^3g^{-1}, which is similar to that of PMO-3, whereas the total pore volume is much lower than for the other samples (table 2). This indicates the collapse of the mesostructure during solvent extraction, which is in agreement with the result of the XRD pattern. The pore wall thickness decreases dramatically when pH>1.2 (Table 2). According to this, the sample synthesized at pH = 2.0 should have the thinnest pore wall among these samples. However, due to collapse of the mesostructure, the pore size of this sample is no longer uniform, as shown by the broad pore size distribution curve in Figure 2. It is known that the template molecules within the pore channel can, to some extent, support the framework of mesoporous materials. This explains why PMO-2 exhibits a well-ordered structure before solvent extraction (Figure 1), while, after template removal, the mesostructure collapses due to the thinned pore wall, evidenced by the broad diffraction peak in the XRD pattern and the disappearance of the clear capillary condensation step in the N_2 adsorption-desorption isotherm.

For the samples synthesized with pH < 1.5, a two-step desorption, which is typical for plugged hexagonal templated silica-like material (PHTS),[26, 27] can be observed in the nitrogen adsorption-desorption isotherms (Figure 2). The first desorption step at high relative pressure can be assigned to the desorption of nitrogen from the open mesopores, while the second desorption step can be attributed to the nanoparticles within the mesopores, narrowing parts of the mesoporous channels, and thus delaying the desorption until the vapor pressure is reduced below the equilibrium desorption pressure from the pore entrances. The two-step desorption becomes quite prominent for PMO-7. The pore-size distribution curves of these samples derived through the desorption branch (Figure S1, Supporting Information) show a bimodal distribution. The first peak can be ascribed to the pore size of the blocked pores (neck size), while the second peak represents the pore size of the open pores. The two-step desorption has been reported for the SBA-15 materials prepared with high SiO_2/P123 ratios, in which the second desorption step is controlled by the pore-blocking effect induced by amorphous SiO_2 nanoparticles.[26] However, in our case, the SiO_2/P123 ratio is constant. Most likely, the acidity of the synthesis mixture is the decisive factor, leading to an excessive polycondensation rate of the silica precursor, relative to the surfactant self-organization. In this case, besides the self-assembling process, the excessive polycondensation of the silica precursor causes the formation of disordered amorphous materials, filling parts of the mesoporous channels.[28, 29] Another prominent feature of the N_2 adsorption-desorption isotherms for the samples synthesized at pH < 1.5 is the second hysteresis loop at a relative pressure larger than 0.80, which implies the existence of secondary mesopores or macropores. It is usually attributed to voids between the primary particles. It can be noticed that the second hysteresis loop becomes more pronounced with decreasing pH value.

Figure 3. *SEM images of solvent-extracted ethane-bridged PMOs synthesized at different pH value: (a) pH=1.8 (PMO-3), (b) pH=1.5 (PMO-4), (c) pH=1.2 (PMO-5), (d) pH=0.8 (PMO-6), (e) pH=0.5 (PMO-7).*

SEM images of the ethane-bridged PMOs synthesized at different pH values are shown in Figure 3. A rice-grain like shape was observed for the samples synthesized with pH ≥ 1.5 (Figure 3a,b), while the particles of the sample synthesized at high acidity (pH < 1.5) exhibit short rod-like morphologies (Figure 3c-e). With increasing acidity, the morphology of the PMO materials becomes less uniform. Besides the rod-like particles, some tiny irregular particulates can be observed, which may be amorphous organosilica species derived from the excessive polycondensation of the silica precursor. Moreover, the aggregation of the particles becomes more obvious at higher acidity, which is probably responsible for the second hysteresis loop in the N_2 adsorption-desorption isotherms. The TEM images and selected area electron diffraction (SAED) pattern of a representative sample, PMO-3, are displayed in Figure 4. The TEM images revealed ordered arrays along the direction perpendicular to the pore axis and the direction of the pore axis, which further confirms the highly ordered 2D hexagonal mesostructure of this material.

Figure 4. *TEM images of solvent-extracted ethane-bridged PMOs synthesized at pH=1.8 (PMO-3) along different directions. The corresponding SAED pattern is presented as inset.*

Comparison of the influence of H_3PO_4 and HCl on the formation of ethane-bridged PMOs

Figure 5. *XRD patterns of ethane-bridged PMOs synthesized with HCl at pH=1.5 (PMO-10) and pH=1.8 (PMO-9). A: as-synthesized samples, B: solvent-extracted samples.*

To compare the influence of polyprotic weak acid H_3PO_4 and strong acid HCl on the synthesis of ethane-bridged PMOs, we also prepared ethane-bridged PMOs with HCl at comparable pH values (pH=2.0, 1.8 and 1.5). The XRD patterns of the samples are shown in Figure 5. For the

sample synthesized at pH=2.0, only an amorphous gel was obtained. The as-synthesized PMO-9 and PMO-10 materials exhibit well-resolved XRD peaks of a highly ordered 2D-hexagonal symmetry (*p6mm*). However, after solvent extraction, PMO-9 exhibits only one broad peak in the low angle region, indicating deterioration of the structural order. The N_2 adsorption-desorption isotherms of solvent-extracted PMO-9 and PMO-10 are shown in Figure S2 (Supporting Information). The isotherm of PMO-10 is of type IV, typical of mesoporous materials, whereas the isotherm of PMO-9 is intermediate between type I and IV, which is similar to that of PMO-2. Most likely, this can be explained by the collapse of the mesostructure during solvent extraction. Moreover, for pH=1.5, the pore size of the PMO synthesized with H_3PO_4 (PMO-4) is larger than for the PMO synthesized with HCl (PMO-10) (Table 2).

In general, when pH>1.5, the polyprotic weak acid (H_3PO_4) favors the formation of highly ordered PMO materials. At the same pH value, the PMOs synthesized with H_3PO_4 have a better ordered structure and larger pore size and surface area than the ones synthesized with HCl. The difference in textural properties may result from different factors. It has been found that the nature of the acidic source has a strong influence on the overall size of the micelles as well as on the whole kinetics of the material formation.[30] Salting-in/chaotropic anions (like Br^-) have a tendency to confine inside the micelles and to reduce their size, whereas salting-out/kosmotropic anions (like $H_2PO_4^-$) give rise to larger micelles.[31, 32] In addition, phosphoric acid quickly deprotonates in water solution with formation of $H_2PO_4^-$. $H_2PO_4^-$ is an excellent buffer, as it can either grab a hydrogen ion and reform phosphoric acid, or it can deprotonate further and becomes monohydrogen phosphate (HPO_4^{2-}). Thus, during the synthesis of ethane-bridged PMOs, the use of H_3PO_4 may, to some extent, keep the pH value of the synthetic system unchanged, and thus result in a better ordered material. Another factor that potentially governs the textural properties

of final material is the interaction between H_3PO_4 and the triblock co-polymer surfactant. The FTIR study of an aqueous mixture containing P123 and H_3PO_4[16] confirmed the interaction between the polar head of the surfactant and H_3PO_4. The phosphate molecules located among the micelles may modify the ionic strength and local pH of the environment and consequently induce a different silica-surfactant interaction type, more related to the N^0I^0 pathway. These factors make H_3PO_4 an excellent acid source for the synthesis of ethane-bridged PMOs with larger pore sizes and surface areas, especially under mild acidic conditions.

Effect of NaCl assistance

Figure 6. *XRD patterns of ethane-bridged PMOs synthesized with the assistance of NaCl (PMO-11 to PMO-13 (Table 1)). A: as-synthesized samples, B: solvent-extracted samples*

The above results show that, by employing H_3PO_4, highly ordered ethane-bridged PMOs can be synthesized at pH<1.8 without the assistance of inorganic salts. When pH=2.0, disordered PMO material is obtained after solvent-extraction. Further decrease of the acidity leads to amorphous gel formation. Inorganic salts have been reported to have a big influence on the formation of mesoporous materials using triblock copolymers as surfactant.[12, 33, 34] It is reported that the addition of inorganic salts can weaken the disturbance of the organic moiety and enhance the self-assembly interaction between the template and the organosilica.[35]

Figure 6 shows the XRD patterns of the sample synthesized at higher pH (pH 2.0 to 2.3) with the assistance of NaCl. For pH=2.0 and 2.1, highly ordered ethane-bridged PMOs are obtained, represented by three well-resolved XRD peaks corresponding to (100), (110) and (200) reflections of 2D hexagonal space group (*p6mm*) (Figure 6). Even for PMO-11 synthesized with pH =2.3 two weak higher order peaks can still be observed, indicating a well-ordered structure.

The intensity of the (100) diffraction peak, however, decreased dramatically. The highly ordered structure have been further confirmed by the TEM images and the SAED patterns shown in Figure S3 (Supporting Information). These XRD and TEM results show that with the assistance of NaCl, well-ordered ethane-bridged PMOs can be synthesized at very low acid concentration. Figure 7 shows the N_2 adsorption-desorption isotherms and the corresponding pore-size distributions of the samples synthesized with the assistance of NaCl. All the isotherms are of type IV with a clear H1-type hysteresis loop characteristic of mesoporous materials. The textural properties are presented in Table 2. It can be noticed that, with the decrease of the acidity, the pore size of the sample increases, while the pore wall thickness decreases.

Figure 7. *(left) N_2 adsorption-desorption isotherms of ethane-bridged PMOs synthesized with the assistance of NaCl (PMO-11 to PMO-13 in Table 1), (right) corresponding pore-size distributions.*

SEM images of PMOs synthesized with the assistance of NaCl are shown in Figure 8. PMO-12 and PMO-13 exhibit rope-like macrostructures, which are made up of parallel running faceted fibers (Figure 8a,b), whereas the morphology of PMO-11 completely shifts from rope-like macrostructures to primarily spherical particles with a diameter of around 3 μm (Figure 8c). The morphology of mesoporous material is to some extent a macroscopic reflection of its mesoscopic symmetry. Considering the hydrophilic/hydrophobic volume ratios (V_H/V_L) which are suggested to account for the formation of different mesophases, especially for nonionic surfactant templating systems, the change of the morphology can be explained by the change of the V_H/V_L ratios. The addition of the NaCl causes the dehydration of EO moieties, leading to a decrease of the hydrophilic volume, and thus decrease the V_H/V_L ratios[36]. Besides, the decrease of the acidity will also lead to a decrease of the V_H/V_L ratios.[12] The change of the V_H/V_L ratios will be more pronounced when both effects exist.

Figure 8. *SEM images of ethane-bridged PMOs synthesized with the assistance of NaCl at different pH value: (a) pH=2.0 (PMO-13), (b) pH=2.1 (PMO-12) and (c) pH=2.3 (PMO-11).*

Direct synthesis of V-containing SBA-15-type PMOs

Figure 9. *XRD patterns of PMO-11 and V-PMO synthesized at pH 2.3. A: as-synthesized samples B: solvent-extracted samples.*

The preparation of metal-containing SBA-15 materials by co-condensation methods is quite difficult due to the strong acidic conditions applied. Under such conditions, the metal species favor their cationic forms, and these cannot be introduced in the framework via co-condensation with the silica precursor. It is reported that the pH value of the synthesis mixture is one of the most important factors in effecting the metal incorporation [37, 38]. We showed in the previous section that, by using a polyprotic weak acid (H_3PO_4) and an inorganic salt (NaCl), SBA-15-type ethane-bridged PMOs can be successfully synthesized under mild acidic conditions (pH=2.3). We now test whether this can be beneficial for the incorporation of metal ions, such as vanadium. For this, $VOSO_4$ was added as vanadium source (see Experimental section for details).

The XRD pattern of the vanadium-containing ethane-bridged PMOs exhibits three well-resolved peaks that are indexed to the (100), (110) and (200) reflections of 2D hexagonal space group (*p6mm*) (Figure 9). It can be noticed that, compared to the vanadium-free PMOs (PMO-11), the XRD peaks of V-PMO shift to lower angles, evidencing an increase of the unit cell parameter. This may indicate a possible substitution of vanadium atoms in the framework of PMO materials due to the fact that the V-O bond is longer than that of Si-O, similar as observed for V-SBA-15[19]. Furthermore, the higher order (110) and (200) peaks of V-PMO become less intense, implying that the long-range structural order of the material is disturbed by the incorporation of

vanadium. As shown in Figure S3 (Supporting Information), the N_2 adsorption-desorption isotherm of V-PMO is of type IV (IUPAC), and exhibits a H1 type hysteresis loop, which is typical for large pore mesoporous materials. The sharp capillary condensation step and the narrow pore size distribution curve further confirm the highly ordered structure of V-PMO. The pore wall thickness of V-PMO is 5.89 nm, which is much larger than that of PMO-11. The increased unit cell parameter and pore wall thickness indicate that vanadium is incorporated into the pore wall of ethane-bridged PMOs.

Figure 10. *(A) DR-UV-Vis spectrum of PMO-11 compared to V-PMO. (B) CW-EPR spectra of solvent-extracted V-PMO recorded at room temperature and 10 K, respectively, and the simulated spectrum.*

The vanadium content of the V-PMO sample is 1.8%, as determined by EPMA (table 2). The vanadium environment is investigated by means of diffuse reflectance UV-Vis and EPR spectroscopy (Figure 10). The UV-Vis spectrum of solvent-extracted V-PMO exhibits three absorption bands centering at 220 nm, 260 nm and 330 nm, respectively. The band at 220 nm is typical for siliceous materials, which can also be observed in the spectra of the vanadium-free PMO-11. The band at 260 nm can be assigned to the low-energy charge transfer associated with V^{5+} species in an isolated tetrahedral coordination possibly with the lattice oxygen, whereas the band at 330 nm corresponds to the polymeric $(V–O–V)_n$ clusters of vanadium species[19, 22, 39]. The band at 330 nm is very weak, indicating that the vanadium mainly exists as isolated species in the PMO materials. Since the vanadium source added to the synthesis mixture was a V^{4+} salt, the UV-Vis result and the white color of the final solid show that most of the V^{4+} has transformed to V^{5+} during the synthesis. However, the CW-EPR spectra of V-PMO evidenced the presence of remaining V^{4+} species. Figure 10B depicted the normalized X-band CW-EPR spectra of solvent-extracted V-PMO recorded at room temperature and 10 K, respectively. At room temperature, the

spectrum is composed of two contributions: a broad line due to dipolarly interacting V^{4+} centers (possibly in $(V–O–V)_n$ clusters), and a multi-line pattern typical of isolated, highly dispersed V^{4+} centers. The latter contribution dominates the EPR spectrum at low temperature. It can be found that the overall shape of this EPR contribution does not change dramatically upon lowering of the temperature, indicating that the corresponding V^{4+} species are completely immobilized in V-PMO. The EPR spectrum at 10K can be simulated using the spin Hamiltonian parameters $g_{x,y}$ = 1.978 (±0.002), g_z = 1.932 (±0.001), $A_{x,y}$ = 205 MHz (±3), and A_z = 548 MHz (±3), which can be attributed to the V^{4+} species in a square-pyramidal coordination, closely resembling the values found for a pentaquovanadyl $[VO(H_2O)_5^{2+}]$.[40] This finding, together with the knowledge that the vanadium center is immobilized, indicates that the isolated, dispersed V^{4+} species are stabilized by the surface silanols and are also ligated to water molecules. According to the UV-Vis and EPR result, it can be concluded that part of the vanadium species exist in a polymeric $(V–O–V)_n$ clusters (possibly embedded in the siliceous matrix), while part of the vanadium species are well dispersed and located on the inner surface of the mesopores, being coordinated to the surface silanols.

4. Conclusion

The effects of the polyprotic weak acid H_3PO_4 and the inorganic salt NaCl on the synthesis of SBA-15-type ethane-bridged PMO materials templated by the copolymer surfactant P123 were investigated. It was found that, compared with HCl, H_3PO_4 is to be preferred for the synthesis of highly ordered ethane-bridged PMO materials with larger pore size and surface areas under mild acidic conditions. With the assistance of H_3PO_4 and NaCl, vanadium-containing SBA-15-type ethane-bridged PMOs were successfully prepared through a direct synthesis approach. The spectroscopic characterization of the V-PMO identified two different types of vanadium sites:

vanadium in $(V–O–V)_n$ clusters most likely part of the framework wall and well dispersed, isolated vanadium-centers immobilized on the inner surface of the mesopores via silanol groups.

5. Acknowledgements

The Erasmus Mundus CONNEC program is acknowledged for PhD funding of F.Lin. Furthermore, the authors acknowledge support by the GOA-BOF project 'Optimization of the structure-activity relation in nanoporous materials', funded by the University of Antwerp.

6. References

[1] B.Y. Guan, Y. Cui, Z.Y. Ren, Z.A. Qiao, L. Wang, Y.L. Liu, Q.S. Huo, Nanoscale, 4 (2012) 6588-6596.

[2] S.S. Park, M.S. Moorthy, C.S. Ha, Npg Asia Mater., 6 (2014).

[3] F. Hoffmann, M. Cornelius, J. Morell, M. Froba, Angew. Chem. Int. Edit., 45 (2006) 3216-3251.

[4] P. Van der Voort, D. Esquivel, E. De Canck, F. Goethals, I. Van Driessche, F.J. Romero-Salguero, Chem. Soc. Rev., 42 (2013) 3913-3955.

[5] M.C. Burleigh, M.A. Markowitz, S. Jayasundera, M.S. Spector, C.W. Thomas, B.P. Gaber, J. Phys. Chem. B, 107 (2003) 12628-12634.

[6] Q.H. Yang, J. Liu, L. Zhang, C. Li, J. Mater. Chem., 19 (2009) 1945-1955.

[7] R.M. Grudzien, B.E. Grabicka, M. Jaroniec, Colloid Surf. A, 300 (2007) 235-244.

[8] X.Y. Bao, X.S. Zhao, X. Li, J. Li, Appl. Surf. Sci., 237 (2004) 380-386.

[9] X.Y. Bao, X.S. Zhao, X. Li, P.A. Chia, J. Li, J. Phys. Chem. B, 108 (2004) 4684-4689.

[10] X.Y. Bao, X.S. Zhao, S.Z. Qiao, S.K. Bhatia, J. Phys. Chem. B, 108 (2004) 16441-16450.

[11] M.C. Burleigh, M.A. Markowitz, E.M. Wong, J.S. Lin, B.P. Gaber, Chem. Mater., 13 (2001) 4411-+.

[12] S.Z. Qiao, C.Z. Yu, Q.H. Hu, Y.G. Jin, X.F. Zhou, X.S. Zhao, G.Q. Lu, Micropor. Mesopor. Mat., 91 (2006) 59-69.

[13] W.P. Guo, J.Y. Park, M.O. Oh, H.W. Jeong, W.J. Cho, I. Kim, C.S. Ha, Chem. Mater., 15 (2003) 2295-2298.

[14] F. Goethals, C. Vercaemst, V. Cloet, S. Hoste, P. Van Der Voort, I. Van Driessche, Micropor. Mesopor. Mat., 131 (2010) 68-74.

[15] M. Colilla, F. Balas, M. Manzano, M. Vallet-Regi, Solid State Sci., 10 (2008) 408-415.

[16] M. Colilla, F. Balas, M. Manzano, M. Vallet-Regi, Chem. Mater., 19 (2007) 3099-3101.

[17] R. Pitchumani, W.J. Li, M.O. Coppens, Catal. Today, 105 (2005) 618-622.

[18] C.M. Chanquia, A.L. Canepa, K. Sapag, P. Reyes, E.R. Herrero, S.G. Casuscelli, G.A. Eimer, Top Catal., 54 (2011) 160-169.

[19] M. Selvaraj, D.W. Park, Appl. Catal. A-Gen, 388 (2010) 22-30.

[20] M. Piumetti, B. Bonelli, P. Massiani, S. Dzwigaj, I. Rossetti, S. Casale, M. Armandi, C. Thomas, E. Garrone, Catal. Today, 179 (2012) 140-148.

[21] J. George, S. Shylesh, A.P. Singh, Appl. Catal. A-Gen, 290 (2005) 148-158.

[22] S. Shylesh, A.P. Singh, Micropor. Mesopor. Mat., 94 (2006) 127-138.

[23] P. Borah, X. Ma, K.T. Nguyen, Y.L. Zhao, Angew. Chem. Int. Edit., 51 (2012) 7756-7761.

[24] S. Stoll, A. Schweiger, J. Magn. Reson., 178 (2006) 42-55.

[25] D.A. Cadenhead, J.F. Danielli, M.D. Rosenberg, Progress in surface and membrane science, 9 (1975).

[26] P. Van Der Voort, P.I. Ravikovitch, K.P. De Jong, M. Benjelloun, E. Van Bavel, A.H. Janssen, A.V. Neimark, B.M. Weckhuysen, E.F. Vansant, J. Phys. Chem. B, 106 (2002) 5873-5877.

[27] P. Van Der Voort, P.I. Ravikovitch, A.V. Neimark, M. Benjelloun, E. Van Bavel, K.P. De Jong, B.M. Weckhuysen, E.F. Vansant, Nanoporous Materials Iii, 141 (2002) 45-52.

[28] C. Vercaemst, M. Ide, H. Friedrich, K.P. de Jong, F. Verpoort, P. Van der Voort, J. Mater. Chem., 19 (2009) 8839-8845.

[29] C. Vercaemst, H. Friedrich, P.E. de Jongh, A.V. Neimark, B. Goderis, F. Verpoort, P. Van Der Voort, J. Phys. Chem. C, 113 (2009) 5556-5562.

[30] S. Manet, J. Schmitt, M. Imperor-Clerc, V. Zholobenko, D. Durand, C.L.P. Oliveira, J.S. Pedersen, C. Gervais, N. Baccile, F. Babonneau, I. Grillo, F. Meneau, C. Rochas, J. Phys. Chem. B, 115 (2011) 11330-11344.

[31] J.L. Blin, M. Imperor-Clerc, Chem. Soc. Rev., 42 (2013) 4071-4082.

[32] S. Manet, A. Lecchi, M. Imperor-Clerc, V. Zholobenko, D. Durand, C.L.P. Oliveira, J.S. Pedersen, I. Grillo, F. Meneau, C. Rochas, J. Phys. Chem. B, 115 (2011) 11318-11329.

[33] C.V. Teixeira, H. Amenitsch, P. Linton, M. Linden, V. Alfredsson, Langmuir, 27 (2011) 7121-7131.

[34] S. Kubo, K. Kosuge, Langmuir, 23 (2007) 11761-11768.

[35] L. Zhang, J. Liu, J. Yang, Q.H. Yang, C. Li, Micropor. Mesopor. Mat., 109 (2008) 172-183.

[36] J.W. Tang, C.Z. Yu, X.F. Zhou, X.X. Yan, D.Y. Zhao, Chem. Commun., (2004) 2240-2241.

[37] Y.Y. Chen, Y.L. Huang, J.H. Xiu, X.W. Han, X.H. Bao, Appl. Catal. A-Gen, 273 (2004) 185-191.

[38] F. Gao, Y.H. Zhang, H.Q. Wan, Y. Kong, X.C. Wu, L. Dong, B.Q. Li, Y. Chen, Micropor. Mesopor. Mat., 110 (2008) 508-516.

[39] S. Shylesh, S.P. Mirajkar, A.P. Singh, J. Mol. Catal. A-Chem, 239 (2005) 57-63.

[40] N.D. Chasteen, In Biological Magnetic Resonance, Berliner, L.; Rueben, J. Eds, Plenum, New York, Vol. 3, p 53 (1981).

Table 1. *Synthetic details of the PMOs under study*

No.	pH	Acid concentration	H_3PO_4/BTEE	P123/BTEE	H_2O/BTEE
PMO-1	2.1	0.48×10^{-3}M	0.16	0.034	336
PMO-2	2.0	0.72×10^{-3}M	0.24	0.034	336
PMO-3	1.8	0.96×10^{-3}M	0.32	0.034	336
PMO-4	1.5	0.19×10^{-2}M	0.64	0.034	336
PMO-5	1.2	0.38×10^{-2}M	1.28	0.034	336
PMO-6	0.8	0.77×10^{-2}M	2.56	0.034	336
PMO-7	0.5	1.54×10^{-2}M	3.84	0.034	336
PMO-8[a]	2.0	*	*	0.034	336
PMO-9[a]	1.8	*	*	0.034	336
PMO-10[a]	1.5	*	*	0.034	336
PMO-11[b]	2.3	0.24×10^{-3}M	0.08	0.034	336
PMO-12[b]	2.1	0.48×10^{-3}M	0.16	0.034	336
PMO-13[b]	2.0	0.72×10^{-3}M	0.24	0.034	336

[a] Materials obtained by tuning pH with 1M HCl. [b] Materials obtained with the assistance of NaCl with a molar ratio of NaCl/BTEE=8

Table 2. *Structural parameters of ethane-bridged PMOs under study*

Sample	*Unit cell parameter a (nm)[a]*	*Surface area(m^2g^{-1})*	*Pore size(nm)[b]*	*Pore Volume (cm^3g^{-1})*	*Micropore volume(cm^3g^{-1})*	*Wall thickness(nm)[c]*
PMO-2	12.03	941	5.76	0.689	0.195	*
PMO-3	11.80	956	7.31	0.941	0.197	4.49
PMO-4	11.84	970	7.03	1.016	0.207	4.81
PMO-5	12.11	891	6.56	0.953	0.160	5.55
PMO-6	12.18	942	6.56	1.098	0.145	5.62
PMO-7	11.98	922	6.32	1.003	0.141	5.66
PMO-9	11.92	917	5.88	0.713	0.152	*
PMO-10	12.05	812	5.09	0.831	0.125	6.96
PMO-11	11.89	839	7.31	0.680	0.226	4.58
PMO-12	11.99	945	7.31	0.941	0.218	4.68
PMO-13	11.85	996	7.03	1.029	0.233	4.82
V-PMO[c]	13.76	850	7.87	0.771	0.203	5.89

[a] Unit cell parameters were calculated using the formula of $a = 2d_{100}/\sqrt{3}$ (*p6mm* symmetry) [b] pore size were calculated from the adsorption branch. [c] pore wall thickness was assessed by subtracting the pore diameter from a [c] V content is 1.8%, determined by EPMA

Figures captions

Figure 1. *XRD patterns of ethane-bridged PMOs synthesized at different pH value ranging from 2.0 to 0.5 (PMO-2 to PMO-7 in Table 1). A: as-synthesized samples, B: solvent-extracted samples.*

Figure 2. *(left) N_2 adsorption-desorption isotherms of ethane-bridged PMOs synthesized at different pH ranging from 2.0 to 0.5 (PMO-2 to PMO-7 in Table 1) and (right) corresponding pore-size distributions.*

Figure 3. *SEM images of solvent-extracted ethane-bridged PMOs synthesized at different pH value: (a) pH=1.8 (PMO-3), (b) pH=1.5 (PMO-4), (c) pH=1.2 (PMO-5), (d) pH=0.8 (PMO-6), (e) pH=0.5 (PMO-7).*

Figure 4. *TEM images of solvent-extracted ethane-bridged PMOs synthesized at pH=1.8 (PMO-3) along different directions. The corresponding SAED pattern is presented as inset.*

Figure 5. *XRD patterns of ethane-bridged PMOs synthesized with HCl at pH=1.5 (PMO-10) and pH=1.8 (PMO-9). A: as-synthesized samples, B: solvent-extracted samples.*

Figure 6. *XRD patterns of ethane-bridged PMOs synthesized with the assistance of NaCl (PMO-11 to PMO-13 (Table 1)). A: as-synthesized samples, B: solvent-extracted samples*

Figure 7. *(left) N_2 adsorption-desorption isotherms of ethane-bridged PMOs synthesized with the assistance of NaCl (PMO-11 to PMO-13 in Table 1), (right) corresponding pore-size distributions.*

Figure 8. *SEM images of ethane-bridged PMOs synthesized with the assistance of NaCl at different pH value: (a) pH=2.0 (PMO-13), (b) pH=2.1 (PMO-12) and (c) pH=2.3 (PMO-11).*

Figure 9. *XRD patterns of PMO-11 and V-PMO synthesized at pH 2.3. A: as-synthesized samples B: solvent-extracted samples.*

Figure 10. *(A) DR-UV-Vis spectrum of PMO-11 compared to V-PMO. (B) CW-EPR spectra of solvent-extracted V-PMO recorded at room temperature and 10 K, respectively, and the simulated spectrum.*

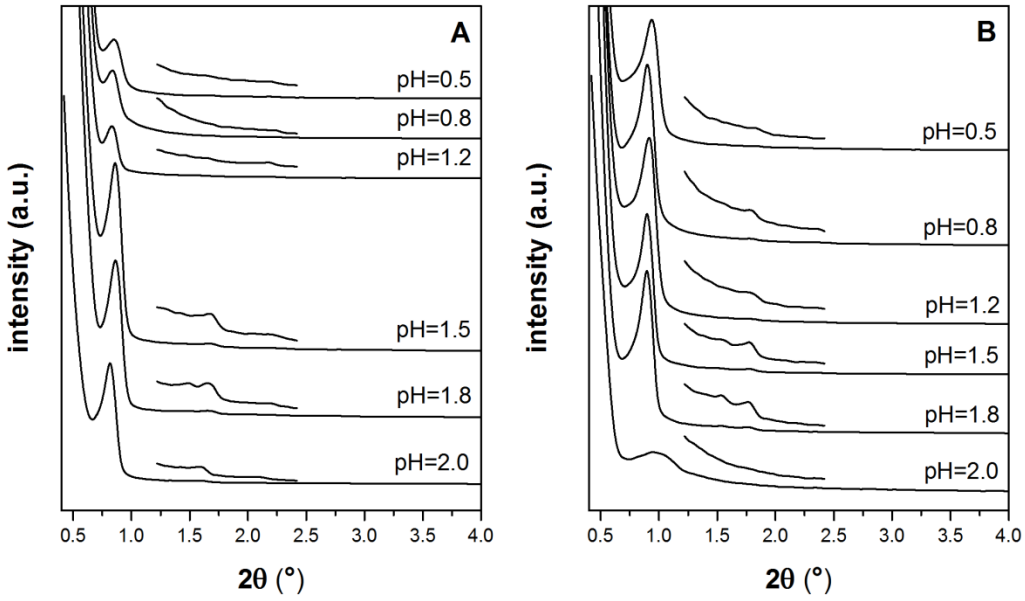

Figure 1. *XRD patterns of ethane-bridged PMOs synthesized at different pH value ranging from 2.0 to 0.5 (PMO-2 to PMO-7 in Table 1). A: as-synthesized samples, B: solvent-extracted samples.*

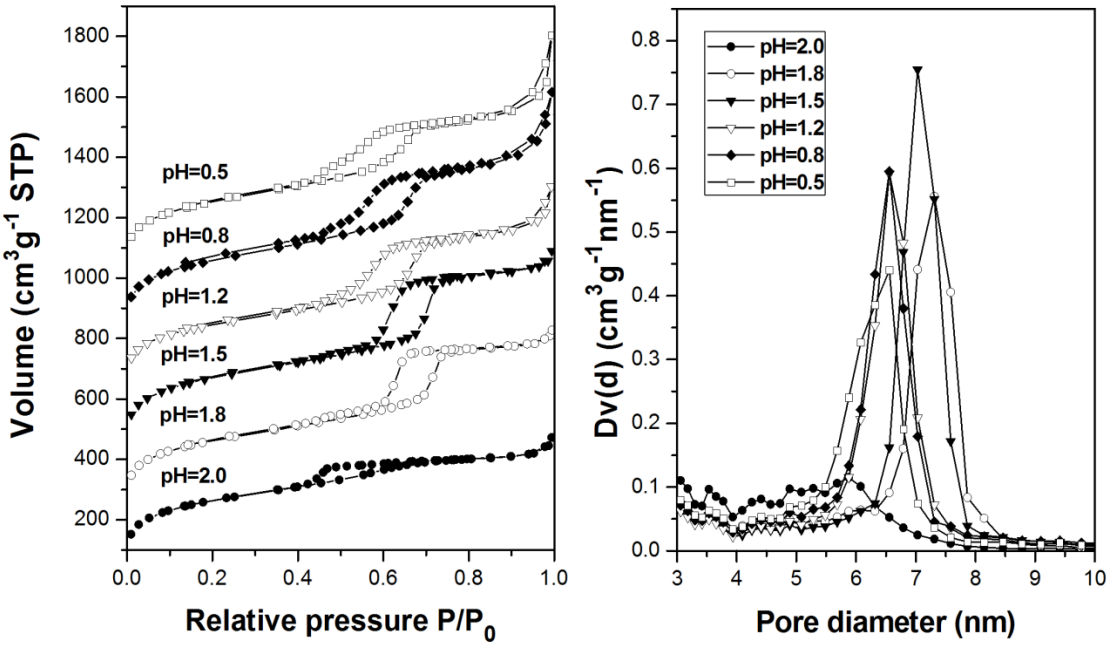

Figure 2. *(left) N_2 adsorption-desorption isotherms of ethane-bridged PMOs synthesized at different pH ranging from 2.0 to 0.5 (PMO-2 to PMO-7 in Table 1) and their corresponding pore size distributions, (right) corresponding pore-size distributions.*

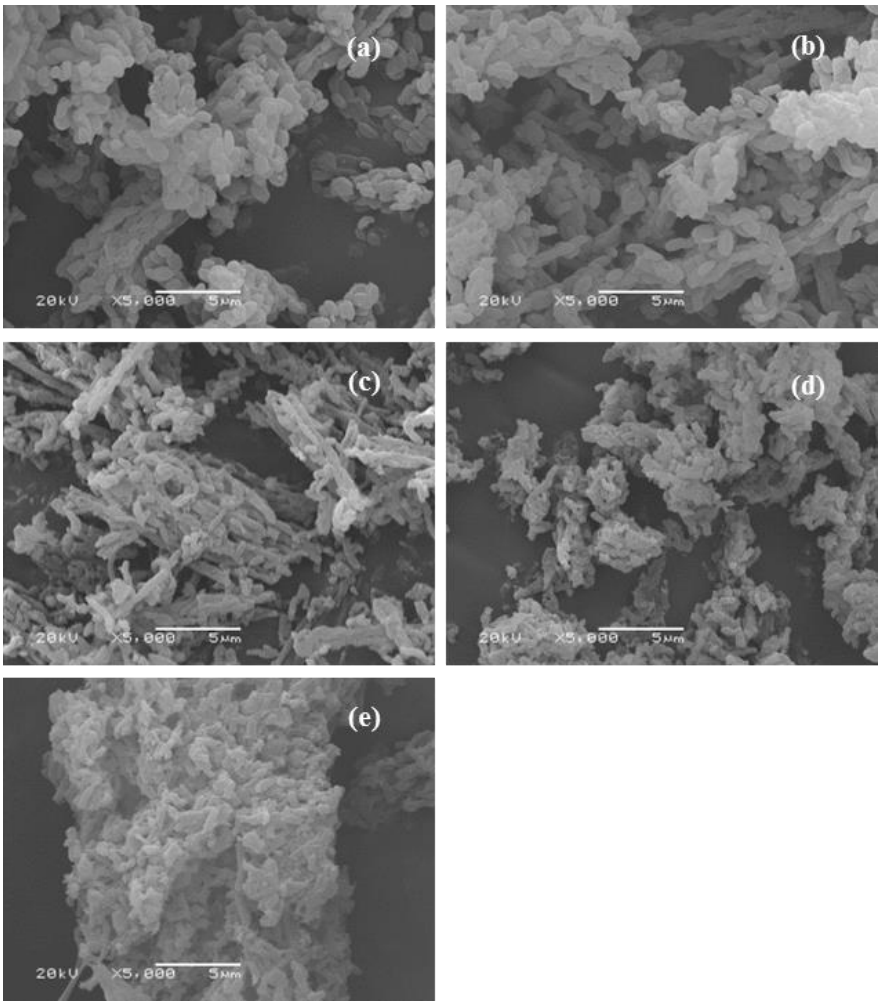

Figure 3. *SEM images of solvent-extracted ethane-bridged PMOs synthesized at different pH value: (a) pH=1.8 (PMO-3), (b) pH=1.5 (PMO-4), (c) pH=1.2 (PMO-5), (d) pH=0.8 (PMO-6), (e) pH=0.5 (PMO-7).*

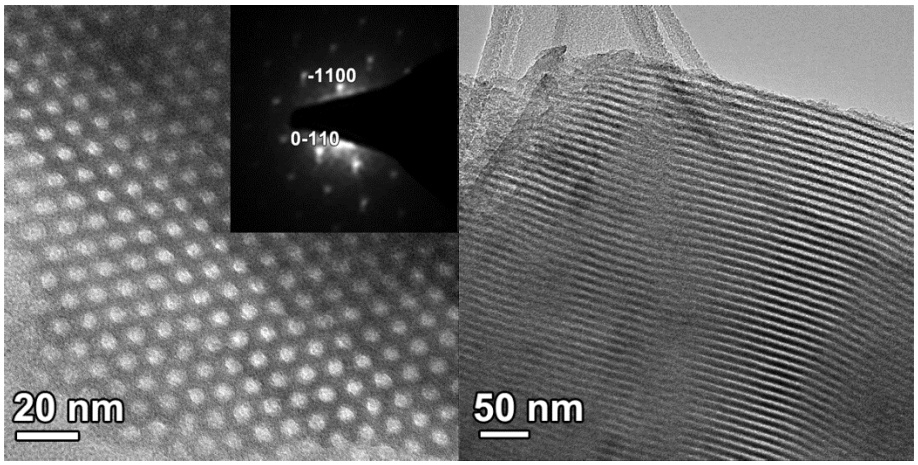

Figure 4. *TEM images of solvent-extracted ethane-bridged PMOs synthesized at pH=1.8 (PMO-3) along different directions. The corresponding SAED pattern is presented as inset.*

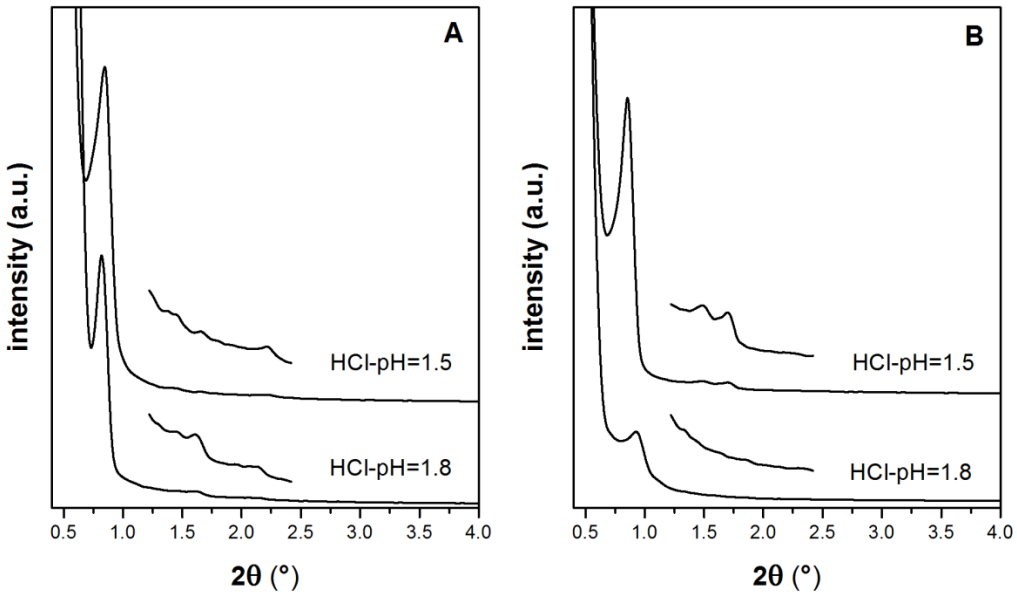

Figure 5. *XRD patterns of ethane-bridged PMOs synthesized with HCl at pH=1.5 (PMO-10) and pH=1.8 (PMO-9). A: as-synthesized samples, B: solvent-extracted samples.*

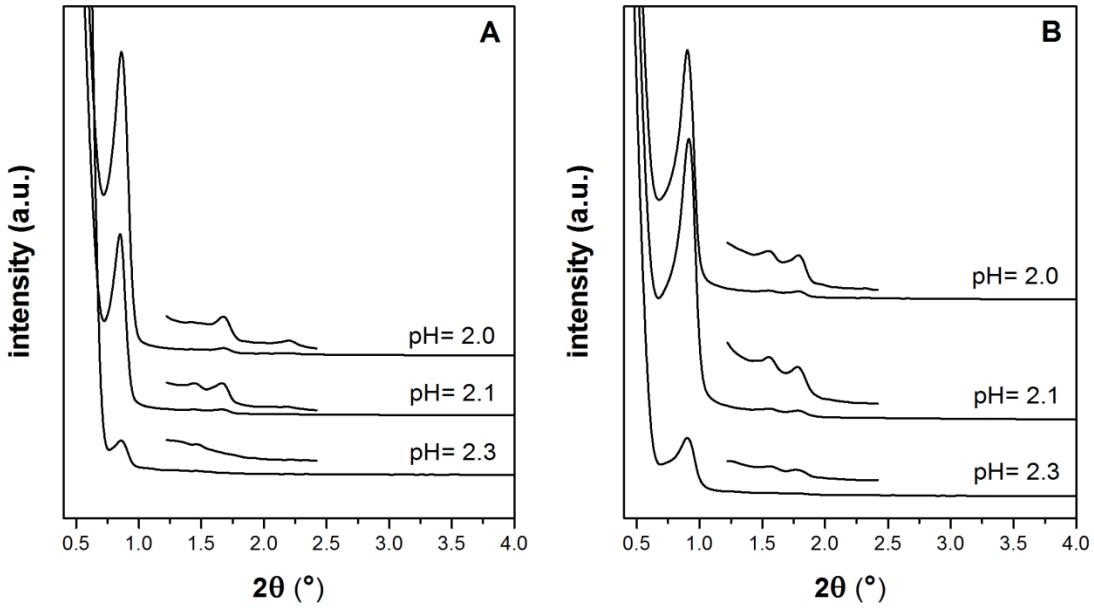

Figure 6. *XRD patterns of ethane-bridged PMOs synthesized with the assistance of NaCl (PMO-11 to PMO-13 (Table 1)). A: as-synthesized samples, B: solvent-extracted samples*

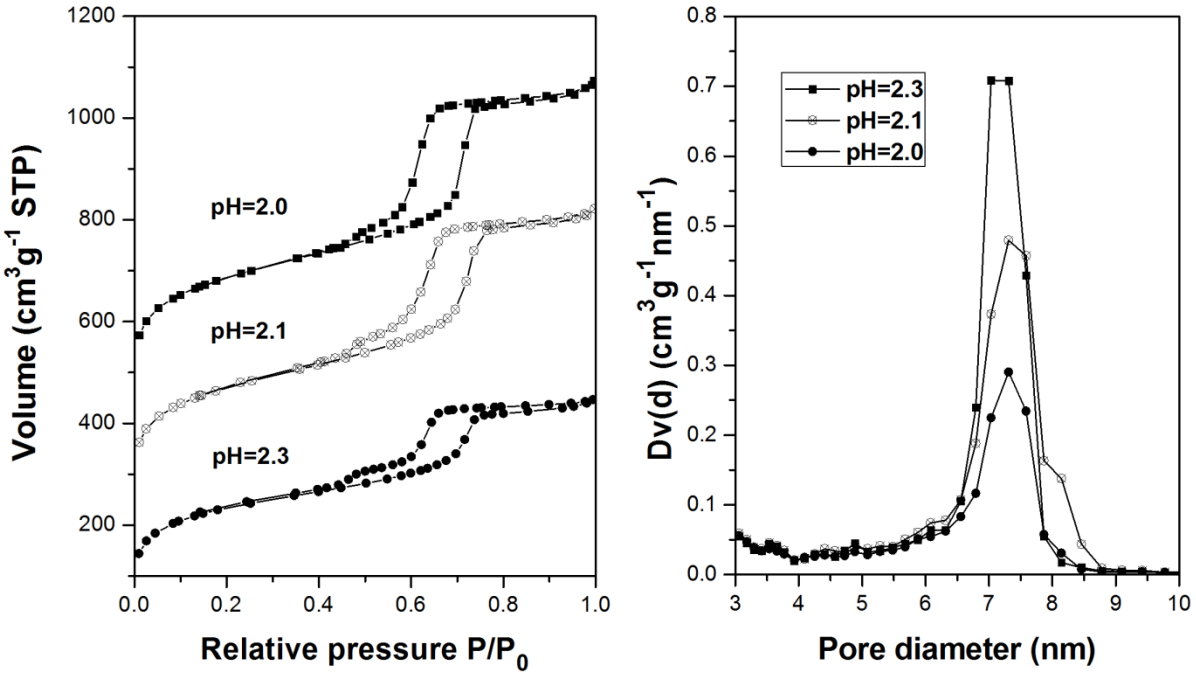

Figure 7. *(left) N_2 adsorption-desorption isotherms of ethane-bridged PMOs synthesized with the assistance of NaCl (PMO-11 to PMO-13 in Table 1), (right) corresponding pore-size distributions.*

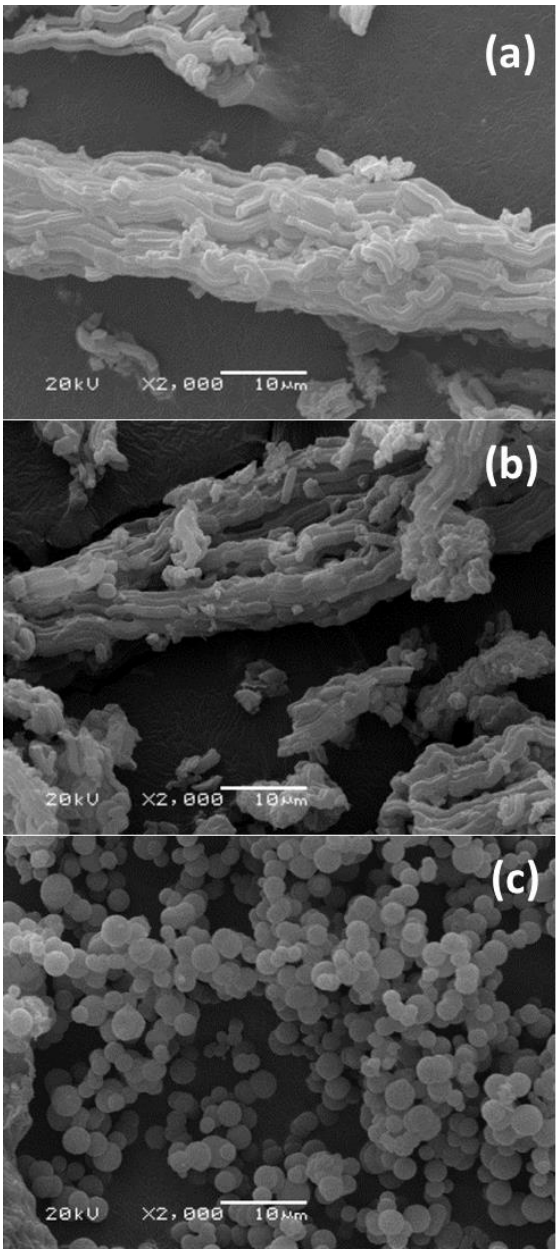

Figure 8. *SEM images of ethane-bridged PMOs synthesized with the assistance of NaCl at different pH value: (a) pH=2.0 (PMO-13), (b) pH=2.1 (PMO-12) and (c) pH=2.3 (PMO-11).*

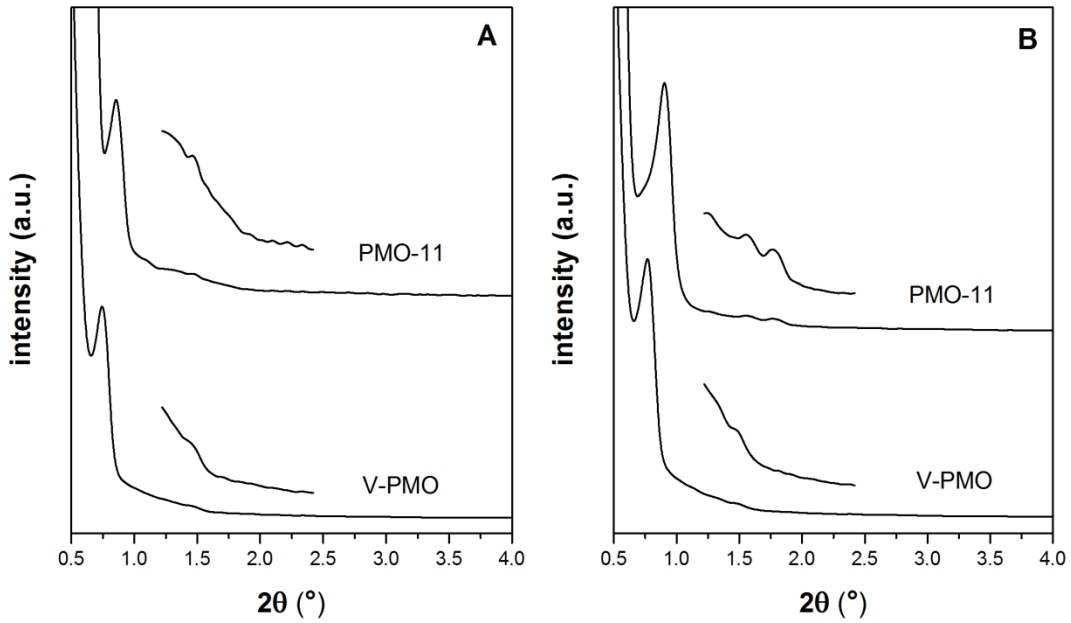

Figure 9. *XRD patterns of PMO-11 and V-PMO synthesized at pH 2.3. A: as-synthesized samples B: solvent-extracted samples*

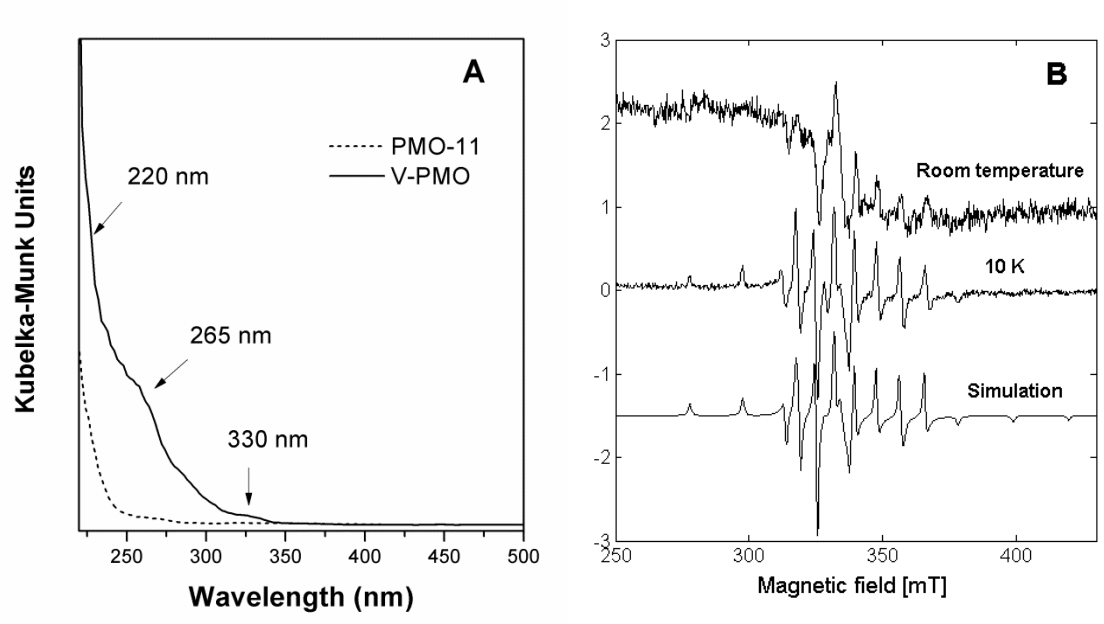

Figure 10. *(A) DR-UV-Vis spectrum of PMO-11 compared to V-PMO. (B) CW-EPR spectra of solvent-extracted V-PMO recorded at room temperature and 10 K, respectively, and the simulated spectrum.*